ChemComm

COMMUNICATION

View Article Online
View Journal | View Issue

Cite this: *Chem. Commun.*, 2026, **62**, 9405

Received 24th March 2026,
Accepted 14th April 2026

DOI: 10.1039/d6cc01759b

rsc.li/chemcomm

Cost-effective nanocubic Prussian blue analogues for enhanced active-barrier epoxy coatings

Xinyue Zhang,†[ac] Chunmei Zhang,†*[b] Mairemu Maihaiti,[a] Kang Ye,[a] Xingzhi He,[c] Lingqian Ye,[c] Minjie Shi,*[ac] Jun Yang[c] and Edison Huixiang Ang*[d]

A cost-effective nanocubic manganese-based Prussian blue analogue with an open framework and redox activity is proposed as an epoxy filler for the first time, demonstrating exceptional active-barrier anticorrosion with an ultralow corrosion rate and durable anticorrosion performance through synergistic physical barrier and interfacial passivation.

Metals are essential to modern society, supporting critical sectors such as infrastructure, transportation, and electronics due to their superior mechanical strength, durability, and stability. However, their inherent susceptibility to corrosion presents ongoing economic, safety, and environmental challenges.[1–3] Protective coatings are among the most widely used and effective strategies to mitigate corrosion.[4,5] Organic coatings, in particular, are favored for their excellent adhesion, chemical resistance, and cost efficiency.[6,7] Nevertheless, their long-term performance is often compromised by environmental degradation or mechanical damage, which diminishes their active-barrier properties. To address these limitations, functional fillers have been incorporated into coating matrices. Conventional additives, such as MXenes, graphene, and related nanomaterials, often require complex synthesis, incur high costs, and exhibit poor dispersibility, leading to aggregation-induced defects that compromise coating integrity.[8–14] There remains a pressing need for novel, cost-effective, and efficient additives capable of simultaneously enhancing the barrier performance and long-term durability of protective coatings.

Prussian blue analogues (PBAs), crystalline coordination materials formed *via* the self-assembly of metal ions and cyanide ligands, feature highly tunable three-dimensional open-framework structures.[15,16] PBAs constitute a large family of cyano-bridged coordination compounds with the general formula $A_xM'_y[M(CN)_6]_{1-y}\cdot nH_2O$, in which the metal species, vacancy concentration, and crystal water content can be readily tuned, leading to diverse framework structures and physicochemical properties.[17,18] Their architecture affords remarkable chemical and thermal stability, while enabling precise control over framework configuration, surface functionalities, and electronic properties through the selection of metal ions (*e.g.*, Fe, Co, Ni, and Mn) and synthesis conditions.[19–22] Among the various PBA compositions, Mn-based PBAs are of particular interest owing to their multiple accessible oxidation states, environmentally benign nature, and promising electrochemical performance,[23–26] which have led to their extensive application in energy storage, environmental remediation, and biomedicine.[27–29] Although PBAs have been widely studied for diverse applications, their potential as functional fillers to enhance protective coatings, especially for corrosion inhibition and interfacial strengthening, has yet to be fully realized.

Herein, we present the first application of nanocubic manganese-based Prussian blue analogues (Mn-PBA) as anticorrosion additives in epoxy (EP) resin. The Mn-PBA nanocubes were synthesized *via* a scalable chemical precipitation method and homogeneously incorporated into the EP matrix to form a Mn-PBA/EP composite coating. After 70 days of immersion in 3.5 wt% NaCl solution, the coating exhibits an ultralow corrosion rate of 6.61×10^{-6} mm a^{-1} and maintains a high low-frequency impedance modulus of 1.23×10^{8} Ω cm^2. The superior corrosion resistance arises from a dual passive–active protection mechanism: the well-dispersed Mn-PBA nanocubes extend the diffusion pathways of corrosive agents, creating a labyrinthine barrier that enhances physical shielding, while their open framework captures Fe^{2+} ions and promotes oxidation to Fe^{3+}, facilitating the formation of a stable passivation layer that suppresses electrochemical corrosion. This study pioneers the use of PBAs in organic coatings, signifying a cost-effective and environmentally

[a] *School of Civil Engineering, Kashi University, Kashi 844000, P.R. China. E-mail: shiminjie@just.edu.cn*
[b] *School of Materials and Chemical Engineering, Henan University of Urban Construction, Pingdingshan 467036, P. R. China. E-mail: 942456323@qq.com*
[c] *School of Materials Science and Engineering, Jiangsu University of Science and Technology, Zhenjiang 212003, P. R. China*
[d] *Natural Sciences and Science Education, National Institute of Education, Nanyang Technological University, Singapore 637616, Singapore. E-mail: edison.ang@nie.edu.sg*
† These authors contributed equally to this work.

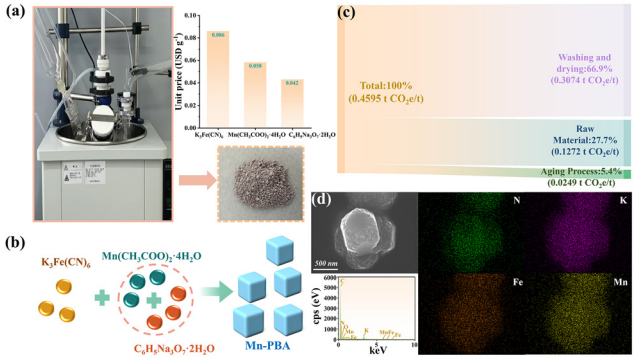

Fig. 1 (a) Synthesis and cost analysis. (b) Formation of Mn-PBA nanocubes. (c) Carbon footprint across each stage. (d) SEM image and the corresponding elemental mapping of Mn-PBA nanocubes.

benign filler that simultaneously improves barrier performance and provides active corrosion inhibition.

As shown in Fig. 1a, the Mn-PBA was successfully synthesized *via* a simple and scalable chemical precipitation route. In this process, a solution of $K_3Fe(CN)_6$ was added dropwise into a mixed solution of $Mn(CH_3COO)_2{\cdot}4H_2O$ and $C_6H_5Na_3O_7{\cdot}2H_2O$ (Fig. 1b), followed by aging at room temperature without external heating or continuous energy input. This method eliminated the need for expensive precursors and avoided conventional high-temperature, high-pressure, or complex purification steps, resulting in low production costs and a minimal carbon footprint (Fig. 1c and Tables S1–S5). These features underscore the method's advantages in cost-effectiveness, environmental sustainability, and suitability for large-scale applications. Morphological and compositional characterization of the as-prepared Mn-PBA was performed using scanning electron microscopy (SEM) and elemental mapping. As shown in Fig. 1d, Mn-PBA exhibits well-defined nanocubic structures with a homogeneous distribution of key elements, reflecting the controlled nucleation and growth during synthesis. The crystal structure of Mn-PBA was further analyzed by X-ray diffraction (XRD, Fig. 2a). The diffraction pattern displays distinct peaks corresponding to the (020), (220), (222), (040), (240), (24-2), (242), (440), and (062) planes of $K_xMnFe(CN)_6{\cdot}yH_2O$, consistent with the monoclinic reference (JCPDS No. 51-1896, space group: $P21/c(14)$). Lattice refinement yields parameters of a = 10.108 Å, b = 10.104 Å, and c = 10.114 Å, with $\alpha = \gamma = 90.0^\circ$ and $\beta = 92.93^\circ$. The inset atomic model illustrates the open-framework architecture, in which Mn and Fe ions are linked *via* cyanide bridges (Mn–N≡C–Fe).

Fourier-transform infrared (FT-IR) spectroscopy further confirms the Mn-PBA structure (Fig. 2b), with characteristic bands at 592 cm^{-1} (Fe–C≡N stretch) and 2059 cm^{-1} (C≡N stretch), while additional bands at 1608 and 3345 cm^{-1} indicate adsorbed and lattice water.[30] X-ray photoelectron spectroscopy (XPS) was used to analyse the chemical composition and oxidation states (Fig. 2c). The N 1s spectrum (Fig. 2d) was deconvoluted into C–N, C≡N, and minor Mn–N contributions. The K 2p spectrum (Fig. 2e) displayed spin–orbit doublets at 293 eV ($2p_{3/2}$) and 296 eV ($2p_{1/2}$). In the Fe 2p region (Fig. 2f),

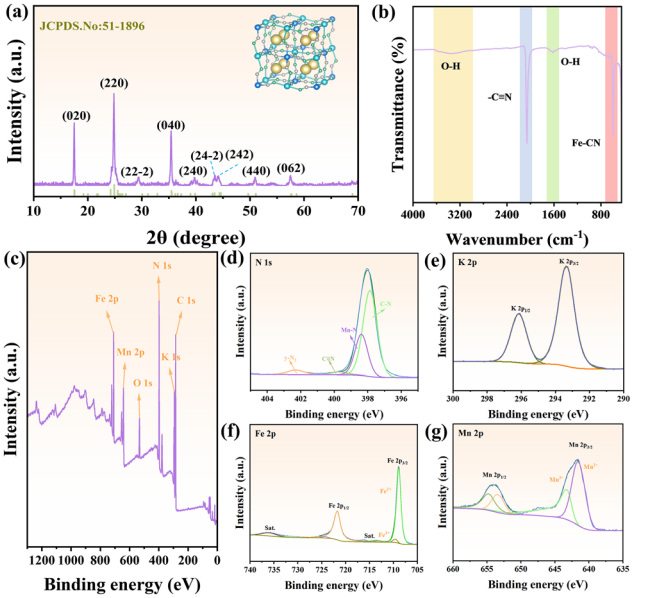

Fig. 2 (a) XRD pattern, (b) FT-IR spectrum, (c) overall XPS spectrum and high-resolution (d) N 1s, (e) K 2p, (f) Fe 2p and (g) Mn 2p spectra of the Mn-PBA.

peaks at 708.88 eV and 721.78 eV correspond to Fe^{2+}, while those at 709.68 eV and 724.28 eV correspond to Fe^{3+}. The Mn 2p spectrum (Fig. 2g) showed peaks at 641.58 eV and 653.48 eV for Mn^{2+}, and at 643.28 eV and 654.88 eV for Mn^{3+}.[31] Deconvolution of the C 1s (Fig. S1) and O 1s (Fig. S2) spectra revealed multiple bonding environments, including C–C, C–N, C≡N, C=O, Mn–O, and O–H species. Collectively, these results confirm the successful synthesis and chemical configuration of Mn-PBA. More importantly, electron paramagnetic resonance (EPR) spectroscopy (Fig. S3) revealed a distinct signal at g = 2.015, attributed to unpaired electrons of Mn^{2+} in a defect-influenced local environment. This observation indicates the presence of Mn-related defect sites within the Mn-PBA framework.[32] The thermal stability of Mn-PBA was further assessed (Fig. S4), demonstrating its suitability as a robust functional filler for protective coatings.

Fig. 3a illustrates the fabrication process of the Mn-PBA/EP coating. A uniform dispersion of Mn-PBA (1% by mass) in EP (Fig. S5) was spin-coated onto a carbon steel substrate to form the composite coating. Mn-PBA was selected as the functional filler because it combines a tunable, defect-rich open framework with facile and scalable synthesis. In addition, its Mn/Fe bimetallic cyanide-bridged structure offers enhanced redox tunability and greater interfacial activity compared to Fe-PBA.[33] For comparison, both pure EP and Mn-PBA/EP coatings were immersed in 3.5 wt% NaCl solution and evaluated electrochemically under ambient conditions.[34] As shown in Fig. 3b, the open circuit potential (OCP) of the Mn-PBA/EP coating (−0.15 V) was significantly more positive than that of the pure EP coating (−0.39 V), indicating improved thermodynamic stability. Ten-week immersion tests (Fig. 3c) further confirm that the OCP of the pure EP coating decreased over time, reflecting progressive corrosion activation, whereas the Mn-PBA/EP coating maintained a stable,

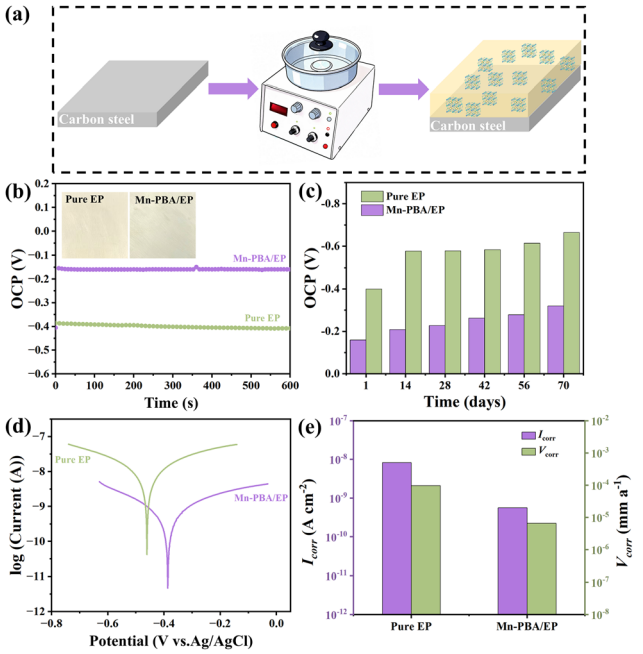

Fig. 3 (a) A diagram of the fabrication of Mn-PBA/EP coating onto Q235 steel through spin coating. (b) OCP curves for pure EP and Mn-PBA/EP coatings. (c) The corresponding OCP evolution over different immersion durations. (d) Polarization curves and (e) the calculated I_{corr} and V_{corr} values for pure EP and Mn-PBA/EP coatings.

relatively positive OCP, demonstrating durable anti-corrosion performance.[35–37] Tafel polarization curves (Fig. 3d and e) were analyzed to derive corrosion potential (E_{corr}) and corrosion current density (I_{corr}). A more positive E_{corr} reflects enhanced electrochemical stability,[38,39] while lower I_{corr} indicates slower corrosion kinetics.[40,41] The Mn-PBA/EP coating exhibited a higher E_{corr} of −0.38 V and an exceptionally low I_{corr} of 5.66×10^{-10} A cm^{-2}, orders of magnitude lower than that of pure EP. Correspondingly, the corrosion rate (V_{corr}) was only 6.61×10^{-6} mm a^{-1}, reflecting the outstanding ability of the coating to impede corrosion propagation. These results validate the superior and long-lasting anti-corrosion performance of the Mn-PBA/EP coating.

Electrochemical impedance spectroscopy (EIS) was performed, and Nyquist and Bode plots were analysed using the equivalent circuit in Fig. S6.[42,43] For the Mn-PBA/EP coating after 70 days of immersion (Fig. 4d–f), the Nyquist semicircle and Bode magnitude plots indicated a high coating resistance ($R_c = 7.12 \times 10^9$ Ω cm^2) and impedance modulus at 0.01 Hz ($|Z|_{0.01Hz} = 6.11 \times 10^9$ Ω cm^2), far exceeding the values of pure EP. Even after prolonged exposure, the Mn-PBA/EP coating maintains $R_c = 6.38 \times 10^7$ Ω cm^2 and $|Z|_{0.01Hz} = 1.23 \times 10^8$ Ω cm^2, confirming sustained barrier integrity. Breakpoint frequency (f_b), representing the onset of coating delamination,[44,45] was consistently low for Mn-PBA/EP (0.032 Hz initially and 6.82 Hz after 70 days), compared with 12.1 Hz for pure EP, highlighting its long-term resistance to failure (Fig. 4g and h).[46–49] A comparison of the properties of Mn-PBA/EP coatings with varying Mn-PBA loadings (0.5%, 1%, and 2%) is presented in Fig. S7. The enhanced corrosion resistance

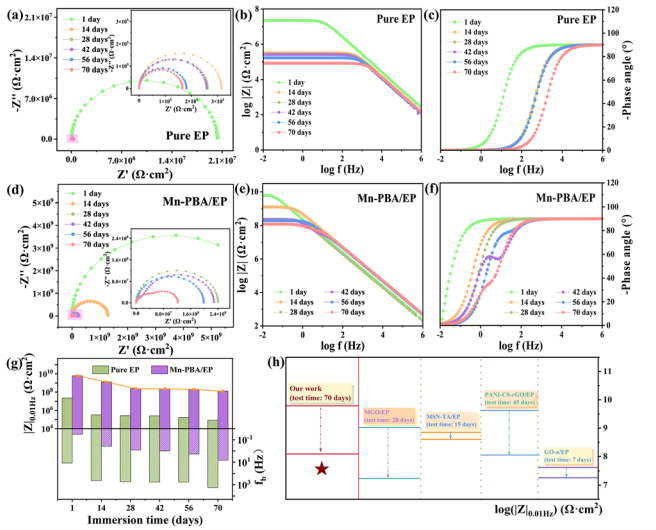

Fig. 4 Nyquist and Bode plots, accompanied by the corresponding phase angle curves of (a)–(c) pure EP and (d)–(f) Mn-PBA/EP coatings after 70 days of immersion in 3.5 wt% NaCl solution. (g) A comparative analysis of the evolution of $|Z|_{0.01Hz}$ and f_b values for pure EP and Mn-PBA/EP coatings from day 1 to day 70 of immersion. (h) Comparative analysis of $|Z|_{0.01Hz}$ values between the Mn-PBA/EP coating and previously reported advanced anti-corrosion coatings.

of Mn-PBA/EP arises from two synergistic mechanisms (Fig. 5a). First, the well-defined cubic lattice of Mn-PBA acts as a robust physical barrier. Its nanocubes fill micropores and defects within the EP matrix (Fig. 5b and c), creating a "labyrinth effect" that extends the diffusion pathways for water, oxygen, and chloride ions, thereby delaying corrosion initiation. Second, the open framework of Mn-PBA actively inhibits corrosion by capturing Fe^{2+} ions at defect sites, which are subsequently oxidized to Fe^{3+} *via* the redox-active $[Fe(CN)_6]^{3-}$ moiety. This facilitates the formation of a stable passivation layer, suppressing both the initiation and propagation of corrosion at the interface. Unlike a simple physical mixture comprising an inert nanoparticle and a soluble redox-active salt, the Mn-PBA employed herein functions as an integrated active-barrier filler, in which the

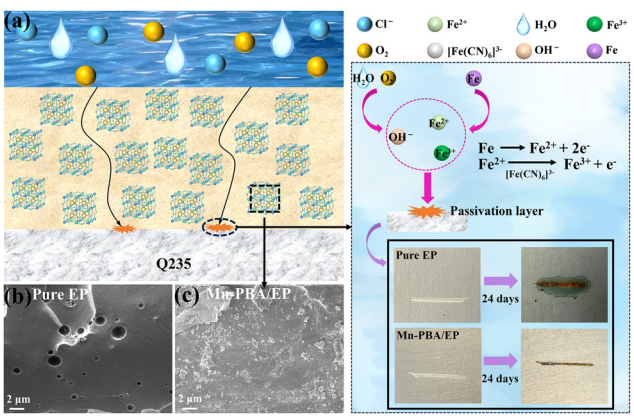

Fig. 5 (a) A schematic illustration of the corrosion protection mechanism of the Mn-PBA/EP coating serving as an anti-corrosion additive. SEM images of (b) pure EP and (c) Mn-PBA/EP coatings.

nanocubic morphology, open-framework structure, and redox-active cyanide-bridged network are unified within a single material. Such an integrated architecture facilitates more uniform dispersion within the EP matrix and preserves the spatial coupling between barrier protection and interfacial activity. In contrast, a physical mixture of SiO_2 and $K_3Fe(CN)_6$ consists of two independent components with distinct dispersion behaviors and interfacial compatibilities. Moreover, unconfined $K_3Fe(CN)_6$ species are more prone to local inhomogeneity, phase separation, and potential leaching within the coating environment.[50,51] Consequently, the preconstructed Mn-PBA framework offers a clear advantage in achieving a stable and durable synergistic anticorrosion effect. The practical applicability of the coating was evaluated under simulated marine conditions using Bohai seawater. Digital images show that, after 1 day, both coatings remained intact, whereas after 24 days, the pure EP coating exhibited visible rust and degradation. In contrast, the Mn-PBA/EP-coated steel remained free of detectable corrosion, even at intentionally scratched sites. The Mn-PBA/EP coating also displays enhanced hydrophobicity (contact angle = 98.9°) compared with pure EP (71.1°, Fig. S8), reducing surface wettability and the adhesion of corrosive species. Corresponding water absorption measurements further support the superior barrier performance of the coating (Fig. S9). As shown in Fig. S10, incorporating Mn-PBA significantly enhances both the adhesion strength and pencil hardness of the EP coating, indicating improved interfacial bonding and mechanical durability.

In summary, we developed a scalable chemical precipitation method to synthesize Mn-PBA nanocubes and demonstrated their effectiveness as functional fillers in enhancing the corrosion protection of epoxy coatings. The nanocubic Mn-PBA not only reinforces the physical barrier of the coating but also, through its open framework and redox-active $[Fe(CN)_6]^{3-}$ moiety, actively captures aggressive species and promotes the formation of a stable passivation film, suppressing both the initiation and propagation of corrosion at the coating–substrate interface. Electrochemical tests after prolonged immersion revealed that the Mn-PBA/EP coating exhibited an ultralow corrosion rate of 6.61×10^{-6} mm a^{-1} and maintained a high low-frequency impedance modulus ($|Z|_{0.01Hz}$) of 1.23×10^8 Ω cm^2 after 70 days of immersion in 3.5 wt% NaCl solution, confirming its robust active-barrier performance. Scratch tests further validated the coating's durability, with no detectable corrosion propagation. This work establishes PBAs as promising active additives and opens a pathway for designing high-performance and long-lasting organic coatings.

Conflicts of interest

There are no conflicts to declare.

Data availability

Data will be made available on request.

Supplementary information (SI): comprehensive synthesis, structural characterization, and electrochemical evaluation of the Mn-PBA anticorrosive filler, along with additional performance data of its epoxy composite coating (Mn-PBA/EP) including water contact angle, water absorption, adhesion strength, pencil hardness, and carbon footprint analysis. See DOI: https://doi.org/10.1039/d6cc01759b.

Acknowledgements

This work was financially supported by the Basic Research Program of Jiangsu (No. BK20251919), the Science and Technology Planning Social Development Project of Zhenjiang City (SJC20240100056 and JC2024018), and the Ministry of Education, Singapore, under the Academic Research Fund (RG88/23).

References

1 T. DebRoy and J. Elmer, *Mater. Today*, 2024, **80**, 737–757.
2 P. Du, Y. Xie, Y. Qiang, X. Li and S. Deng, *Corros. Sci.*, 2025, **245**, 112676.
3 F. Seidi and D. Crespy, *Chem. Commun.*, 2020, **56**, 11931–11940.
4 S. Jose, Z. Lapierre, T. Williams, C. Hope, T. Jardin, R. Rodriguez and P. Menezes, *Coatings*, 2025, **15**, 878.
5 Y. Wu, Y. Wu, Y. Sun, W. Zhao and L. Wang, *Adv. Mater.*, 2024, **36**, 2312460.
6 S. Zhang, X. Hei, C. Hu, T. Li, Y. Shen and K. Ren, *Chem. Eng. Sci.*, 2026, **323**, 123219.
7 S. Zhang, C. Wang, H. Liu, Q. Niu, Q. Yin, Z. Wang, Z. Liu and H. Wang, *Chem. Eng. Sci.*, 2025, **317**, 122009.
8 Y. Ning, D. Jian, S. Liu, F. Chen, Y. Song, S. Li and B. Liu, *Carbon*, 2023, **202**, 20–30.
9 J. Ding, H. Zhao and H. Yu, *ACS Nano*, 2022, **16**, 710–720.
10 F. Jiang, W. Zhao, Y. Wu, J. Dong, K. Zhou, G. Lu and J. Pu, *Prog. Org. Coat.*, 2019, **127**, 70–79.
11 A. Kumar, J. Jose and M. Hussein, *Prog. Org. Coat.*, 2022, **163**, 106678.
12 J. Wang, W. Tan, H. Yang, X. Rao, X. Luo, L. Ma, C. Ren, A. Mol and D. Zhang, *npj Mater. Degrad.*, 2023, **7**, 39.
13 X. Li, X. Chen, J. Chen, D. Huo, X. Gao, J. Dong, Y. Yin, J. Liu and D. Nan, *Prog. Org. Coat.*, 2024, **194**, 108624.
14 Y. Xie, Y. Wu, X. Zhao, H. Ma, P. Zhang and Y. Zhang, *Chem. Eng. Sci.*, 2025, **313**, 121715.
15 Z. Wei, W. Zhao, J. Hu, T. Deng and N. Zhang, *Chem. Commun.*, 2024, **60**, 396–399.
16 K. Du, Y. Liu, Y. Zhao, H. Li, H. Liu, C. Sun, M. Han, T. Ma and Y. Hu, *Adv. Mater.*, 2024, **36**, 2404172.
17 X. Wu, Y. Ru, Y. Bai, G. Zhang, Y. Shi and H. Pang, *Coord. Chem. Rev.*, 2022, **451**, 214260.
18 M. Jiang, T. Li, X. Wei, W. He, Y. Li, F. Xu, Y. Ma, Y. Zhang and J. Wang, *J. Energy Chem.*, 2026, **118**, 169–177.
19 Y. Kumar, S. Sana, T. Ramachandran, M. Assiri, S. Rao and S. Kim, *Dalton Trans.*, 2024, **53**, 10770.
20 L. Xu, Y. Liu, M. Chen, W. Wu, S. Qiu, H. Wu, M. Zheng, X. Zhang and X. Wu, *Chem. Eng. Sci.*, 2025, **302**, 120848.
21 J. Peng, W. Zhang, Q. Liu, J. Wang, S. Chou, H. Liu and S. Dou, *Adv. Mater.*, 2022, **34**, 2108384.
22 B. Xie, Z. Wang, T. Gao, Q. Guo, Y. Tan, X. Chen and W. Wang, *Small*, 2025, **21**, e08865.
23 Y. Liu, H. Liu, R. Zhang, Y. Zhong, Z. Wu, X. Wang and Z. Zhang, *Ionics*, 2024, **30**, 39–59.
24 C. Ding, Z. Chen, C. Cao, Y. Liu and Y. Gao, *Nano-Micro Lett.*, 2023, **15**, 192.
25 W. Shu, C. Han and X. Wang, *Adv. Funct. Mater.*, 2024, **34**, 2309636.
26 B. Zhao, Y. Wang, Z. Wang, Y. Hu, Y. Zhang and J. Bai, *Chem. Eng. J.*, 2024, **487**, 150437.
27 H. Zheng, G. Zhang, B. Yan and H. Pang, *Adv. Funct. Mater.*, 2025, **36**, e22461.
28 R. Wang, C. Qian, Z. Zhang, H. Shen, J. Xia, D. Cui, K. Sun, H. Liu, C. Guo, F. Yu, J. Li and W. Bao, *Small*, 2023, **19**, 2206848.

29 Y. Liu, S. Fan, Y. Gao, Y. Liu, H. Zhang, J. Chen, X. Chen, J. Huang, X. Liu, L. Li, Y. Qiao and S. Chou, *Small*, 2023, **19**, 2302687.
30 M. Jiang, Y. Zhao, Z. Hou, T. Li, X. Wei, F. Wu, F. Xu, F. Kang and J. Wang, *ACS Energy Lett.*, 2025, **11**, 526–536.
31 Y. Tang, W. Li, P. Feng, M. Zhou, K. Wang, Y. Wang, K. Zaghib and K. Jiang, *Adv. Funct. Mater.*, 2020, **30**, 1908754.
32 Y. Shang, X. Li, J. Song, S. Huang, Z. Yang, Z. Xu and H. Yang, *Chemistry*, 2020, **6**, 1804–1818.
33 H. Fu, X. Wang, J. Yang, Z. Wu, H. Ren, J. Ji, M. Shi and E. Ang, *Chem. Sci.*, 2026, **17**, 968.
34 Y. Ren, B. Li and J. Zhang, *Nanoscale Horiz.*, 2026, **11**, 855–864.
35 Y. Hao, S. Liu, L. Song and Y. Shen, *J. Appl. Polym. Sci.*, 2025, **142**, e57374.
36 M. Cai, H. Yan, Y. Li, W. Li, H. Li, X. Fan and M. Zhu, *Chem. Eng. J.*, 2021, **410**, 128310.
37 Z. Li, J. Wang, Y. Dong, D. Xu, X. Zhang, J. Wu, T. Gu and F. Wang, *J. Mater. Sci. Technol.*, 2021, **71**, 177–185.
38 K. Auepattana-Aumrung, T. Phakkeeree and D. Crespy, *Prog. Org. Coat.*, 2022, **163**, 106639.
39 B. Li, H. Yang, J. He, S. Yu, R. Xiao, H. Luo, Y. Wen, S. Peng, X. Liao and D. Yang, *Materials*, 2023, **16**, 2015.
40 P. Xiao, N. Chen, J. Liu, L. Yang, D. Chen and M. Shi, *Prog. Org. Coat.*, 2024, **186**, 108017.
41 C. Li, Z. Xia, H. Yan, Q. Shi and J. Weng, *Corros. Sci.*, 2022, **199**, 110150.
42 L. Cao, R. Wang, W. Wang, X. Yuan, J. Wei, D. Han, Y. Chen, Y. Pei, W. Li and S. Chen, *Prog. Org. Coat.*, 2026, **21**, 109709.
43 S. Liu, X. Zhang, C. Wang, C. Yin, J. Rao, Y. Zhang and D. Losic, *J. Magnesium Alloys*, 2025, **13**, 1050–1065.
44 J. Ding, H. Zhao and H. Yu, *Chem. Eng. J.*, 2022, **430**, 132838.
45 L. Pei, D. Lin, S. Yuan, R. Lu, Z. Bai, Y. Sun, Y. Zhu, Y. Jiang, J. Zhu and H. Wang, *Chem. Eng. J.*, 2023, **457**, 141158.
46 X. Li, X. Chen, J. Chen, D. Huo, X. Gao, J. Dong, Y. Yin, J. Liu and D. Nan, *Prog. Org. Coat.*, 2024, **194**, 108624.
47 J. Wang, W. Tan, H. Yang, X. Rao, X. Luo, L. Ma, C. Ren, A. Mol and D. Zhang, *npj Mater. Degrad.*, 2023, **7**, 39.
48 A. M. Kumar, J. Jose and M. A. Hussein, *Prog. Org. Coat.*, 2022, **163**, 106678.
49 F. Jiang, W. Zhao, Y. Wu, J. Dong, K. Zhou, G. Lu and J. Pu, *Prog. Org. Coat.*, 2019, **127**, 70–79.
50 X. Liu, X. Han, M. Wang, D. Wang, G. Fei, A. Chen and X. Lai, *Prog. Org. Coat.*, 2024, **191**, 108407.
51 F. Xie and D. Dreisinger, *Hydrometallurgy*, 2007, **88**, 98–108.